A Power Flow Diagnostic Framework for Multi-Domain Dynamic Systems with Application to Drive-by-Wire Ground Vehicles

S. Ganta and J. Wagner, Ph.D., P.E.
Department of Mechanical Engineering
Clemson University, Clemson, South Carolina 29634

Abstract

The emergence of drive-by-wire (DBW) ground vehicles offers the opportunity for improved vehicle responsiveness, human-machine interface features, and environmental friendliness by permitting computer-controlled assistance. Multiple domain electro-mechanical components such as electronic throttle control (ETC), steer-by-wire (SBW), and brake-by-wire (BBW) replace the traditional mechanical and fluid linkages with sensors, actuators, and real-time computer control. From a safety perspective, these critical subsystems must provide reliable operation achieved through continual on-board monitoring to promptly detect degradations. This paper presents a model based power flow diagnostic (PFD) strategy to comprehensively monitor DBW subsystems to detect hard failures that degrade the vehicle's overall transient behavior. The diagnostic strategy has been applied to the ETC, SBW, and BBW subsystems in stand-alone and integrated configurations. A broad combination of twenty-three electrical and mechanical parameter anomalies have been explored to validate the diagnostic strategy. The real-time residuals reflected the system behavior during the simulated failure scenarios; the Chi-Square statistical test consistently and accurately registered threshold violations. Representative results are presented and discussed to demonstrate the performance of the diagnostic algorithm.

1. Introduction

A global approach to diagnostic/prognostic strategies in multi-domain dynamic systems, such as DBW vehicles, can facilitate the design of a comprehensive automotive health monitoring algorithm. The increasingly stringent norms being established by the Environmental Protection Agency on fuel efficiency and tailpipe emissions, as well as the need for onboard diagnostics, requires the existence of sophisticated control algorithms to ensure vehicle compliance. The emerging application of servo-motor driven actuators in transportation systems is partially due to environmental requirements in addition to their enhanced operational flexibility within a computer controlled architecture. A vehicle architecture (refer to Fig. 1) with integrated DBW technology can offer design flexibility, improved emissions, and enhanced safety [7, 10].

Integrating DBW systems can offer significant automobile performance enhancements but raise new safety issues (e.g., failure modes). For successful integration, system issues such as reliability and fail-safe computer controlled operation must be addressed [1]. In general, failure diagnostic methods must perform three tasks: detection, isolation, and estimation. A number of process diagnostics surveys have been written [3, 5, 6, 12] that introduce fundamental principles. Although the majority of current on-board automotive diagnostic algorithms may be categorized as model-free, opportunities exist to apply model-based strategies that incorporate mathematical models for the physical system [4]. Some of the model-based diagnostic strategies include observer based method, parameter estimation, and parity space. In spite of the benefits of analytical redundancy, issues such as model inaccuracy, plant variance, and noise need to be addressed to ensure operational integrity.

The aforementioned drawbacks, and the need to encompass the diagnosis of multiple subsystems operating in unison under a comprehensive monitoring strategy, presents new challenges. Although the signal analysis methods have been examined in-depth, the actual architecture of the diagnostic/prognostic strategy has not received great attention. Rather, a "silo" approach has been pursued in which individual, dedicated, diagnostics are developed for each subsystem and not integrated in a unified manner for harmonious system health monitoring. The gradual integration of automobile operations under an "umbrella" control algorithm mandates commensurate evolution of diagnostic strategies to ensure the units operate in a cohesive manner. This paper is organized as follows. Section 2 discusses the power flow diagnostic strategy. Section 3 presents the ETC, SBW, and BBW models. The application of the proposed monitoring strategy to the DBW subsystems and the simulation results are presented in Section 4. The conclusion is provided in Section 5.

2. Power Flow Diagnostic Strategy

From a high-level perspective, a plant may be considered to be composed of various subsystems that operate in a unified manner. Such a subsystem framework generally involves collaborative and/or independent operations to achieve the desired end results (refer to Fig. 2). The system dynamics are also influenced by exogenous factors that have to be fully considered. Consequently, the real-time control algorithms must regulate the subsystem power flows. These power flows may hence provide a basis for the real-time diagnosis of individual components operating in an integrated plant environment. An

underlying premise is that (A.1) abnormal power consumption shall indicate faulty subsystem operation and facilitate diagnosis.

Figure 1: Vehicle configuration incorporating drive-by-wire systems

The proposed power flow diagnostic strategy ensures overall integrity of the plant functionality through a synchronized integration of documented "no-failure" system operational information (i.e., *a priori* knowledge) into the existing mathematical analysis (refer to Fig. 3). The strategy combines physical models, *a priori* operating databases, Kalman Filters/observers, statistics, and hypothesis testing. The technical approach is based on the real-time monitoring between interacting systems with *a priori* knowledge compared to generate the power flow residuals. The ideal subsystem power flows are computed from *a priori* information databases that are referenced to operating indices having high correlations with subsystem power flows. The use of *a priori* plant operating information provides the opportunity to "tune" the diagnostic strategy based on the local plant performance.

The subsystem governing variables (i.e., state and exogenous) that have a high correlation may be determined from experimental procedures (or physical models when available) and indexed to operating databases during normal (i.e., "no failure") operation to develop multi-dimensional reference surfaces. The empirical relationships should meet the prescribed accuracy, or error, tolerances.

Figure 2: Power flow interactions within a multiple domain dynamic system

A six-phase process is proposed to create a power flow monitoring strategy:

I. Identify the subsystem governing variables (i.e., $\left(\underline{x}_i(t), \underline{\upsilon}_i(t)\right)$) to use as indices to reference the corresponding power during "no failure" operations

II. Map the governing variables to corresponding power flows utilizing *a priori* plant operating knowledge contained in the function, $\hat{p}_i(t) = g_{pi}(.)$.

III. Perform real-time monitoring of measurable signals (e.g., state variables, pressure, temperature, etc.) through direct sensor data acquisition and/or estimation of unavailable state variables for any system operating point. Supply the variables to the *a priori* database to generate the ideal power flows, $\hat{p}_i(t)$, and calculate the actual power flow, $p_i(t)$.

IV. Compute the residual, $e_i = p_i - \hat{p}_i$. The generated power flow residuals are assumed to have certain intrinsic qualities (i.e., statistical properties) under the null hypothesis of normal system operations. The underlying assumptions include:

A.2 The dependent variables (i.e., power flows) vary with the independent variables (i.e., subsystem governing variables) in a systematic fashion.

A.3 The generated residuals, e_i, may be corrupted by system noise (i.e., probability distributions such as Gaussian, binomial, or exponential).

A.4 Co-variances, Σ, of the residuals will be zero.

V. Estimate the subsystem dynamic variability, $R^2 = \sum_{i=1}^{N} \frac{(\hat{p}_i - \bar{p})^2}{(p_i - \bar{p})^2}$, to determine the "fit" of the developed model. The variables p, $\hat{p}$, and $\bar{p}$

denote the actual, estimated, and average power flow variable values. The square of the correlation between the actual and the estimated power flows provides $0 \leq R^2 \leq 1$ where $R^2 = 1$ implies a perfect fit. The term $\bar{p}$ can be estimated as $\bar{p} = \frac{1}{N} \sum_{j=1}^{N} p_j$.

VI. Establish "failure free" characteristics for the diagnostic threshold references (i.e., power flow variance information for each system) to adjust the fault detection sensitivity required

$$\left\{ \begin{array}{ll} \chi^2 \leq \chi^2_{(q-1),\alpha} & : \text{No Fault} \\ \chi^2 > \chi^2_{(q-1),\alpha} \text{ , for } \Delta t_c > \Delta t_{th} & : \text{Fault} \end{array} \right\} \quad (1)$$

where Δt_c denotes the time period the Chi-Square value violates the threshold and Δt_{th} is the period that must be exceeded to flag a fault (refer to Fig. 4).
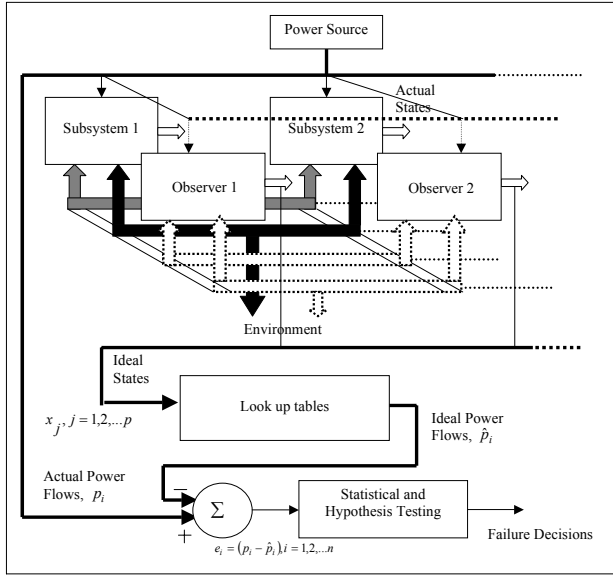
Figure 3: High level representation of diagnostics

Under the null hypothesis (H$_o$) of "no-failure" and assuming Gaussian noise, the sum of normalized square innovations, χ_i^2, would be given by $\chi_i^2 = \frac{(q-1)\sigma_i^2}{\sigma_{io}^2}$ where the sample and population variances are

$$\sigma_i^2 = \frac{1}{(q-1)} \sum_{j=k-q+1}^{k} \left(e_{ij} - \bar{e}_i \right)^2 \text{ and } \sigma_{io}^2 = \frac{1}{(N)} \sum_{j=k-q+1-N}^{k-q} \left(e_{ij} - \bar{\mu}_i \right)^2 ,$$

respectively. The term e_{ij} denotes the residual sample of the ith subsystem for $i = 1,2,...,n$ subsystems. Note that

$$\bar{e}_i = \frac{1}{q} \sum_{j=k-q+1}^{k} e_{ij} \text{ and } \bar{\mu}_i = \frac{1}{N} \sum_{j=k-q+1-N}^{k-q} e_{ij} .$$

The sensitivity of the failure detection depends on the length of the residual vector; "q" represents the number of residuals for the given subsystem (i.e.,

$e \in \Re^q$). In addition, an adjustable confidence threshold (i.e., level of significance, α) ensures tailoring of alarm sensitivity.
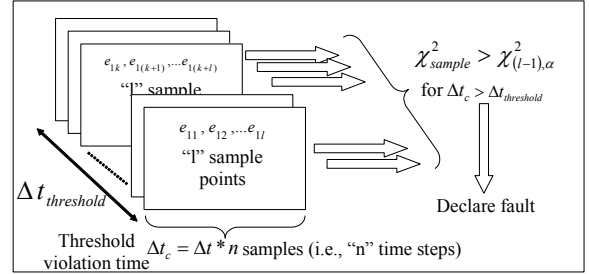
Figure 4: Threshold violation for anomalous behavior

3. X-by-Wire System Modeling

For greater design flexibility, operational reliability, and safety, conventional mechanical, hydraulic, and pneumatic transportation systems such as transmissions, steering systems, and brakes have been upgraded to electrically actuated systems. Consequently, closed-loop control laws dictate system functionality based on the situational awareness gauged from on-board sensors. In this section, ETC, SBW, and BBW models are presented.

3.1 Electronic Throttle Control System

The electro-mechanical dynamic system model, shown in Fig. 5, describes the normal "no failure" ETC hardware operation [2]. The ETC system uses a torque motor to rotate the throttle plate between $0 < \theta < \pi/2$ radians (i.e., closed to wide-open throttle). The governing equations for the dc servo-motor and throttle body are:

Throttle DC servo-motor:

$$\frac{di_a}{dt} = \left(\frac{1}{L_a} \right) \left(-R_a i_a - K_b N \frac{d\theta}{dt} + e_a \right) \quad (2)$$

Throttle body:

$$\frac{d^2\theta}{dt^2} = \left(\frac{1}{N^2 J_m + J_g} \right) \left(-\left(N^2 b_m + b_t \right) \frac{d\theta}{dt} + N T_m - k_{sp} \left(\theta + \theta_0 \right) - T_a \right) \quad (3)$$

The airflow over the throttle plate induces a torque, $T_a = R_{af} \Delta P A_p \cos^2 \theta$, with the exogenous variable $\Delta P = \left(P_{atm} - P_m \right)$ and $A_p = \pi R_p^2$. The manifold pressure is a nonlinear throttle angle dependent function, $P_m = f\left(\theta, P_{atm}, N \right)$, that approaches atmospheric pressure as the throttle approaches a wide-open state.

3.2 Steer-by-Wire System

The SBW system integrates the directional assembly and driver interface under microprocessor control by removing the conventional direct steering column linkage (refer to Fig. 6). The driver interface includes the steering wheel and column, and a low torque dc servo-motor for haptic interface [8]. The directional control

assembly differs from the conventional rack and pinion system since a high torque servo-motor displaces the rack. The governing dynamics for the SBW system are:
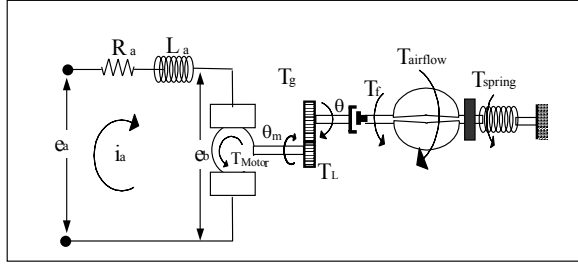
Figure 5: Throttle-by-wire system diagram

Steering wheel:

$$\frac{d^2\theta_{sw}}{dt^2} = \frac{1}{J_{sw}}\left(T_{driver} - b_{sc}\left(\frac{d\theta_{sw}}{dt} - \frac{d\theta_{m1}}{dt}\right) - k_{sc}\left(\theta_{sw} - \theta_{m1}\right)\right) \quad (4)$$

Driver interface motor shaft:

$$\frac{d^2\theta_{m1}}{dt^2} = \frac{1}{J_{m1}}\left(\begin{array}{c} -b_{m1}\dfrac{d\theta_{m1}}{dt} - b_{sc}\left(\dfrac{d\theta_{m1}}{dt} - \dfrac{d\theta_{sw}}{dt}\right) - \\ k_{sc}\left(\theta_{m1} - \theta_{sw}\right) + T_{m1} \end{array}\right) \quad (5)$$

Driver interface DC servo-motor:

$$\frac{di_{a1}}{dt} = \frac{1}{L_{a1}}\left(-R_{a1}i_{a1} - K_{b1}\frac{d\theta_{m1}}{dt} + e_{a1}\right) \quad (6)$$

Directional control assembly servo-motor:

$$\frac{di_{a2}}{dt} = \frac{1}{L_{a2}}\left(-R_{a2}i_{a2} - K_{b2}\frac{d\theta_{m2}}{dt} + e_{a2}\right) \quad (7)$$

Directional control assembly motor shaft:

$$\frac{d^2\theta_{m2}}{dt^2} = \frac{1}{J_{m2}}\left(-b_{m2}\frac{d\theta_{m2}}{dt} - k_{S2}\left(\theta_{m2} - \frac{y_{rack}}{r_{pinion}}\right) + T_{m2}\right) \quad (8)$$

Directional control assembly rack:

$$\frac{d^2y_{rack}}{dt^2} = \frac{1}{m_{rack}}\left(\begin{array}{c} -2k_L\left(y_{rack} - r_L\delta_F\right) - b_{rack}\dfrac{dy_{rack}}{dt} + \\ \dfrac{k_{S2}}{r_{pinion}}\left(\theta_{m2} - \dfrac{y_{rack}}{r_{pinion}}\right) - F_{fr,rack} \end{array}\right) \quad (9)$$

Road wheel:

$$\frac{d^2\delta_F}{dt^2} = \frac{1}{J_{zw}}\left(-b_{kp}\frac{d\delta_F}{dt} + k_L r_L\left(y_{rack} - r_L\delta_F\right) - T_{fr,rack} - M_z\right)$$
$$(10)$$

where $T_{fr,rack}$ is the nonlinear kingpin friction torque and M_z is the aligning torque at the road wheel interface.

3.3 Brake-by-Wire System

The BBW system operates by actuating the brake caliper using a servo motor to enable the brake pads to engage the rotor and induce a brake torque on the wheels

(refer to Fig. 7). The driver's commands and brake pad position feedback signal are processed by the BBW controller to regulate the servo-motor voltage [9]. The BBW system can be integrated with the existing power train control module (PCM) to enable traction control and antilock braking [7]. The governing dynamics for the dc servo-motor and brake pad assembly are:

Brake system DC servo-motor:

$$\frac{d^2\theta_m}{dt^2} = \left(\frac{1}{J_m}\right)\left(-b_m\left(\frac{d\theta_m}{dt}\right) - T_L + T_m\right) \quad (11)$$

Brake assembly dynamics:

$$\frac{d^2x}{dt^2} = \left(\frac{1}{J_{eq}}\right)\left(-B_{eq}\left(\frac{dx}{dt}\right) - \left(\frac{t_r}{A_r}\right)\left(F_{brake} + F_{sp}\right) + NK_ti_a\right) \quad (12)$$

where $\quad J_{eq} = \left(\dfrac{2\pi N^2 A_r J_m}{p} + \dfrac{t_r m_{p2}}{A_r} + t_r A_r m_{p1}\right) \quad$ and

$B_{eq} = \left(\dfrac{2\pi N^2 A_r b_m}{p} + \dfrac{t_r b_{p2}}{A_r} + t_r A_r m_{p1}\right)$, respectively.

A stiff spring ensures that the brake calipers are held in position against the rotor. The spring has been initialized to a displacement x_0 which produces a force $F_{sp} = K_{p2}(x - x_0)$. The brake caliper piston displacement induces the force $F_{brake} = K_{brake}x$.
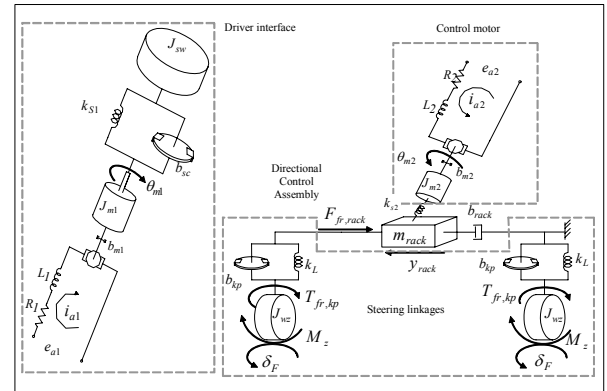
Figure 6: Steer-by-wire system [8]

4. Application of the Diagnostic Strategy

The numerical simulations of the drive-by-wire systems have been completed using Matlab/Simulink™. A fourth order Runge-Kutta scheme with a time step of Δt=1.0e-3 seconds has been selected. This is followed by the application of the PFD strategy to detect plant failures. White noise has been introduced to assess the diagnostic strategy when noise corrupts the plant measurements.

™ Matlab and Simulink are registered trademarks of The Mathworks, Natick, MA

4.1 Fault Free Approach

The application of the PFD strategy is illustrated using the ETC system. This is accomplished by first developing an *a priori* database of "no-failure" ETC system operations. As per Phase I, the governing variables (i.e., "through" and "across" variables) contributing to the power flow are obtained as

$$p_1 = g_{p1}\left(\theta, d\theta/dt, \Delta P\right) = v_1 * i_1 \qquad (13)$$

In Phase II, the ETC power flow information was extracted from the numerical simulations and indexed against the throttle angular displacement, θ, and the angular velocity, $d\theta/dt$, for various pressure differentials, ΔP, to obtain the *a priori* database.
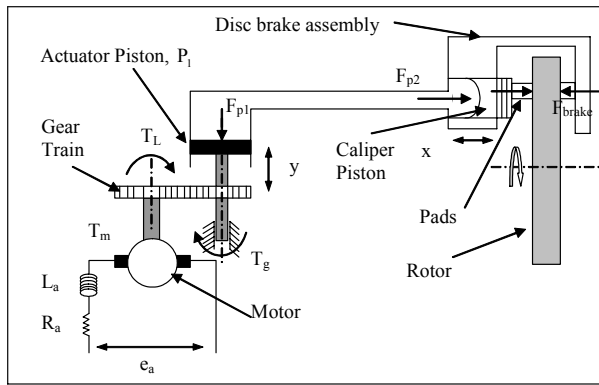
Figure 7: Brake-by-wire system diagram

For the present analysis, the governing variables (i.e., θ, $d\theta/dt$, and ΔP) were directly obtained from the system simulations and supplied to the diagnostic block (i.e., Phase III). The power flow residual was computed, as per Phase IV, for an ETC system input that resulted in a sine wave throttle plate displacement of amplitude $0 < \theta < \pi/2$ and frequency f=0.17 Hz. The power flow residual varied between -1.05 Watts to 0.75 Watts. The discrepancy may be attributed to the empirical nature of ideal power flow estimation in addition to the system noise which corrupts the plant measurements.

The dynamic variability of the subsystem was computed (Phase V) which yielded R^2=0.979. This is indicative of the empirical power flow model accuracy and implies that the ETC dynamics are largely accounted for by the database information. The final task (Phase VI) establishes the failure free characteristics for the diagnostic threshold reference to adjust the fault detection sensitivity. The system operating information (i.e., power flow residual data) was accrued during the initial stages of the simulation (e.g., during simulation time t<60 seconds) to obtain the baseline operating characteristics to compute the population system variance. This was obtained as $\sigma_0^2 = 0.1264$ for fault free system operation.

A series of residual samples were collected (e.g., a sample size of 100 residual data points for every time step of Δt=1s during simulation time t>60s) to compute the sample variance, followed by the Chi-Square hypothesis test using the population variance information. The information was then updated for every time step till a fault was detected (as per the criteria stated in Section 2). The threshold was set at 90% (i.e., significance level of $\alpha = 10\%$). This threshold can be adjusted during the calibration process to tailor the diagnostic robustness. The test results are shown in Fig. 8. It can be observed that the Chi-Square value does not exceed the upper control limit (i.e., $\chi^2_{(99,0.1)}$ or UCL=117.407) during the fault free simulation. Similarly, the PFD strategy was applied to the SBW and BBW systems to generate the baseline operating characteristics.
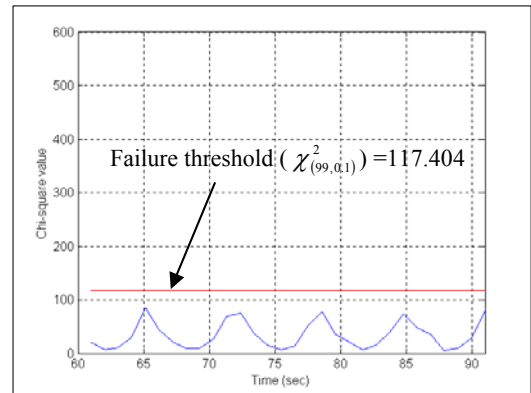
Figure 8: Chi-Square test for the fault free ETC system

4.2 Individual System Faults

The evaluation of the diagnostic strategy for common system failures will be completed by manipulating the corresponding model parameters at time t=70 seconds during each simulation (refer to Table 1). The time period the Chi-Square value has to exceed the threshold for a failure to be flagged has been set by trial and error to Δt_{th}=2s. Faults 1.1 and 2.3 will be discussed to be brief.

In Fig. 9, the ETC subsystem simulation results are displayed when Fault 1.1 (i.e., motor torque coefficient) of 10% magnitude decrease was introduced. The introduction of the fault causes a "surge" in the ECU power flow (i.e., 20.6%) due to the increased demand on the motor (i.e., greater current draw) required to compensate for the reduced motor torque generated at time t>70 seconds. The corresponding power flow residual ranged from 0.22W to 7.83W. This anomaly was promptly detected with the Chi-Square test flagging a fault at t=72s. Note that the Chi-Square value exceeds the threshold at t=70s, but sustained violations for periods of Δt_c=4s (i.e., $\Delta t_c > \Delta t_{th} = 2s$) were observed at t>70 seconds (i.e., a detection delay of $\Delta t_d = 2s$.

In Fig. 10, the results from the simulation of the SBW directional assembly when Fault 2.3 (i.e., motor damping coefficient) of magnitude 25% increase was introduced are displayed. The power flow residual varied

between -5.28W to 8.58W, and the Chi-Square test flagged a fault at t=73s (i.e., $\Delta t_d = 3$s).

Test	System	Fault	Magnitude	Detection	Test	System	Fault	Magnitude	Detection
1.1	**ETC**	Motor torque	-10%	√	2.1	**SBW-DA**	Motor torque	-10%	√
1.2		Motor resistance	+30%	√	2.2		Motor Resistance	+15%	√
1.3		Motor damping	+30%	√	2.3		Motor damping	+25%	√
1.4		Throttle damping	+55%	√	2.4		Rack damping	+100%	
1.5		Back EMF	+100%		2.5		Rack stiffness	+5%	√
1.6		Return spring	-20%	√	2.6		Position sensor bias	+5%	√
1.7		Position sensor bias	+20%	√	4.1	**BBW**	Motor torque	-5%	√
3.1	**SBW-DI**	Motor torque	-10%	√	4.2		Motor Resistance	+15%	√
3.2		Motor Resistance	+45%	√	4.3		Motor damping	+40%	√
3.3		Motor compliance	-2%	√	4.4		Back EMF	+100%	
3.4		Motor damping	+30%	√	4.5		Brake pad	+5%	√
					4.6		Position sensor bias	+10%	√

Table 1: Suite of drive-by-wire representative system faults to evaluate diagnostic algorithm

4.3 Integrated System Faults

The performance of the PFD strategy was evaluated when two or more drive-by-wire systems operate in unison per the two test cases listed in Table 2. A detailed vehicle simulation model with the BBW, SBW, and ETC subsystems incorporated into an eight DOF chassis model was the platform. Test 1 is presented to showcase the power flow diagnostic strategy's robustness.
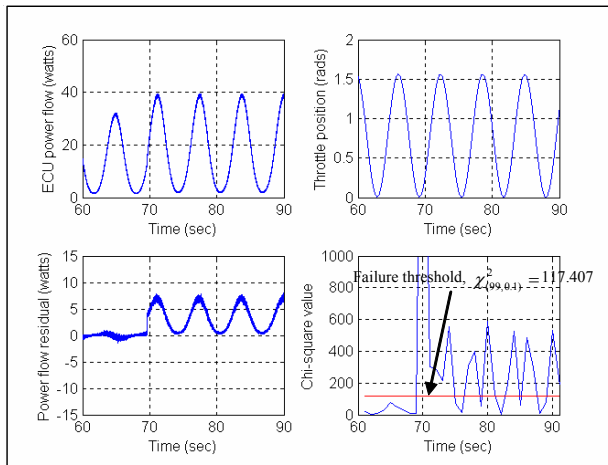
Figure 9: Electronic throttle control system with Fault 1.1 of magnitude 10% decrease introduced at t=70s

Test 1 focuses on a vehicle maneuver involving a sinusoidal steer input with a faulty BBW system engaging a single wheel (e.g., due to a general BBW controller malfunction). The test procedure allows the diagnostic strategy to check for subsystem discrepancies,

if any, in spite of different vehicle handling characteristics. A dry level road surface, $\mu_{road} = 0.85$, with an initial vehicle velocity of u=56 kph has been considered. A BBW system, Fault 4.2 of magnitude 15% engages the rear left tire at time t=70s).
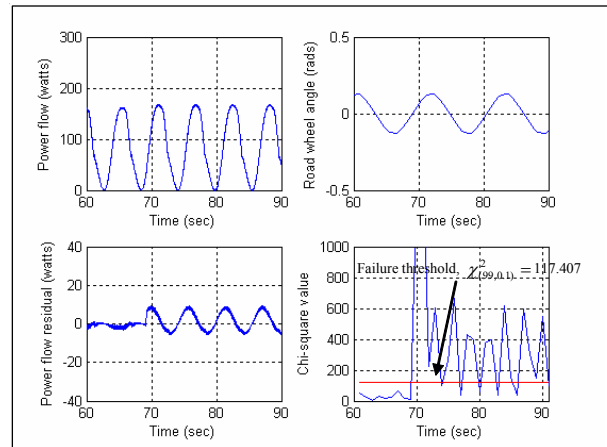
Figure 10: Steer-by-wire system with Fault 2.3 of magnitude 25% increase introduced at t=70s

The simulation results of the SBW system are shown in Fig. 11. The power flow residual ranged between -2.72W and 1.45W with the Chi-Square value not exceeding the threshold. Fig. 12 shows the simulation results for the BBW system. Note that no brakes are applied prior to t=70s. The PFD strategy correctly deciphered the faulty BBW system with the power flow residual ranging between 2.16W and 9.25W, and the Chi-Square test flagging a fault at t=73s (i.e., $\Delta t_d = 3$s).

	ETC		SBW		BBW	
	Fault	No Fault	Fault	No Fault	Fault	No Fault
T-1		√		√	4.2	
T-2	1.2			√		√

Table 2: Integrate drive-by-wire vehicle test case matrix
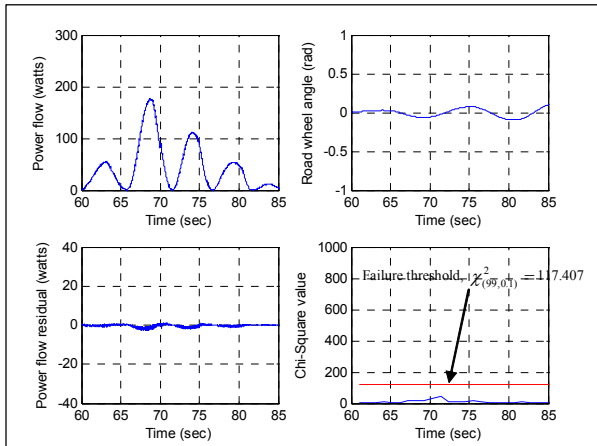
Figure 11: SBW simulation results for integrated drive-by-wire system Fault 4.2 of BBW system at t=70s

5. Conclusion

A power flow diagnostic strategy for automotive drive-by-wire systems, operating in an integrated vehicle environment, has been developed. A series of automotive systems have been modeled and analyzed; the governing dynamics were integrated into an eight degree-of-freedom chassis model with nonlinear tire dynamics to develop a comprehensive simulation. The diagnostic algorithm was successfully implemented and validated using a series of failure scenarios. The simulation results demonstrated that the health monitoring strategy can successfully detect degraded system behavior when relevant fault magnitudes were inserted. In the future, a hardware-in-the-loop bench (e.g., [11]) will be created.

References

1. Achenbach W., "Safety Concepts in X-by-Wire Systems," SAE paper no. 2002-21-0030, 2002.

2. Conatser, R., Wagner, J., Ganta, S., and Walker, I., "Diagnosis of Automotive Electronic Throttle Control Systems," *J. Control Engineering Practice*, vol. 12, no. 1, pp. 23-30, 2004.

3. Frank, P. M., "Fault Diagnosis in Dynamic Systems Using Analytical and Knowledge-based Redundancy—A Survey and Some New Results," proc. IFAC Symposium on Advanced Information Processing in Automatic Control, pp. 457-459, 1990.

4. Gertler, J. J., "Survey of Model-Based Failure Detection and Isolation in Complex Plants," *IEEE Control Systems Mag.*, vol. 8, no. 9, pp. 3-10, 1988.

5. Huo, Y., Ioannou, A., and Mirmirani, M., "Fault Tolerant Control and Reconfiguration for High Performance Aircraft: Review," Center for Advanced Transportation Technologies, University of Southern California, CATT Technical Report 01-11-01, 2001.

6. Isermann, R., "Process Fault Detection Based on Modeling and Estimation Methods - A Survey," *Automatica*, vol. 20, no. 4, pp. 387-404, 1984.

7. Jonner, D., Winner, H., Dreilich, L., and Schunck, E., "Electro-Hydraulic Brake System: The First Approach to Brake-by-Wire Technology," SAE paper no. 960991, 1996.

8. Mills, V., and Wagner, J., "Behavioral Modeling and Analysis of Hybrid Vehicles Steering Systems," *Proceedings of the Institution of Mechanical Engineers, Part D, Journal of Automobile Engineering*, vol. 217, no. 5, pp. 349-361, 2003.

9. Semmler, S., Isermann, R., Schwarz., R., and Rieth, P., "Wheel Slip Control for Antilock Braking Using Brake-by-Wire Actuators," SAE paper no. 2003-01-0325, 2003.

10. Stanton, N., and Marsden, P., "Drive-By-Wire Systems: Some Reflections on the Trend to Automate the Driver Role," *Proceedings of the Institution of Mechanical Engineers, Part D: Journal of Automobile Engineering*, vol. 211, no. D4, pp. 267-276, 1997.

11. Wagner, J., and Keane, J., "A Strategy to Verify Chassis Controller Software", *IEEE Transactions on Systems, Man, and Cybernetics, Part A: Systems and Humans,* vol. 27, no. 4, pp. 480-493, 1997.

12. Willsky, A. S., "A Survey of Design Methods for Failure Detection in Dynamic Systems," *Automatica*, vol. 12, no. 6, pp. 601-611, 1976.

Figure 12: BBW with Fault 4.2 of magnitude 15% increase introduced at t=70s for integrated DBW system